ACCOUNTS
of chemical research

The Story of a Monodisperse Gold Nanoparticle: $Au_{25}L_{18}$

JOSEPH F. PARKER, CHRISTINA A. FIELDS-ZINNA, AND ROYCE W. MURRAY*

Kenan Laboratories of Chemistry, University of North Carolina at Chapel Hill, Chapel Hill, North Carolina 27599

RECEIVED ON MARCH 17, 2010

CONSPECTUS

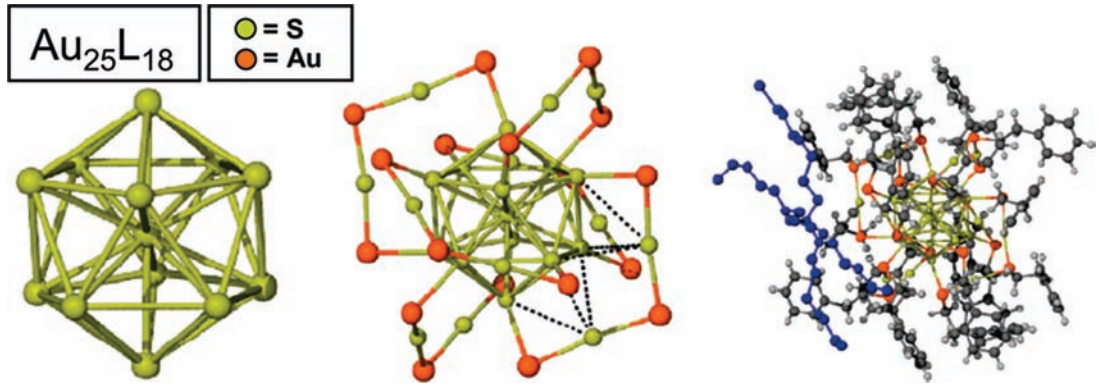

Au nanoparticles (NPs) with protecting organothiolate ligands and core diameters smaller than 2 nm are interesting materials because their size-dependent properties range from metal-like to molecule-like. This Account focuses on the most thoroughly investigated of these NPs, $Au_{25}L_{18}$. Future advances in nanocluster catalysis and electronic miniaturization and biological applications such as drug delivery will depend on a thorough understanding of nanoscale materials in which molecule-like characteristics appear. This Account tells the story of $Au_{25}L_{18}$ and its associated synthetic, structural, mass spectrometric, electron transfer, optical spectroscopy, and magnetic resonance results. We also reference other Au NP studies to introduce helpful synthetic and measurement tools.

Historically, nanoparticle sizes have been described by their diameters. Recently, researchers have reported actual molecular formulas for very small NPs, which is chemically preferable to solely reporting their size. $Au_{25}L_{18}$ is a success story in this regard; however, researchers initially mislabeled this NP as $Au_{28}L_{16}$ and as $Au_{38}L_{24}$ before correctly identifying it by electrospray-ionization mass spectrometry. Because of its small size, this NP is amenable to theoretical investigations. In addition, $Au_{25}L_{18}$'s accessibility in pure form and molecule-like properties make it an attractive research target.

The properties of this NP include a large energy gap readily seen in cyclic voltammetry (related to its HOMO−LUMO gap), a UV−vis absorbance spectrum with step-like fine structure, and NIR fluorescence emission. A single crystal structure and theoretical analysis have served as important steps in understanding the chemistry of $Au_{25}L_{18}$. Researchers have determined the single crystal structure of both its "native" as-prepared form, a $[N((CH_2)_7CH_3)_4^{1+}][Au_{25}(SCH_2CH_2Ph)_{18}^{1-}]$ salt, and of the neutral, oxidized form $Au_{25}(SCH_2CH_2Ph)_{18}^{0}$. A density functional theory (DFT) analysis correctly predicted essential elements of the structure. The NP is composed of a centered icosahedral Au_{13} core stabilized by six $Au_2(SR)_3$ semirings. These semirings present interesting implications regarding other small Au nanoparticle clusters. Many properties of the Au_{25} NP result from these semiring structures.

This overview of the identification, structure determination, and analytical properties of perhaps the best understood Au nanoparticle provides results that should be useful for further analyses and applications. We also hope that the story of this nanoparticle will be useful to those who teach about nanoparticle science.

Published on the Web 07/02/2010 www.pubs.acs.org/acr
10.1021/ar100048c

Introduction

The strong organothiolate−gold bond has spawned three major research arenas, starting with self-assembled monolayers (SAMs) on planar Au surfaces, which have been objects of numerous surface chemistry investigations. Two more recent fields involve Au nanoparticles, one being the thiolation of large citrate-protected Au colloids with ensuing biomedically oriented studies,[1] and the other being very small (diam < 3 nm) thiolated Au NP prepared in the early work of Brust et al.[2] and Whetten et al.[3] This laboratory's interest in small Au nanoparticles[4] was captured in recognizing the need to better chemically define these materials and by ensuing results on size-dependent electrochemical properties and the alteration and functionalization of their ligand shells. The metal-to-molecule transition was being encountered in these thiolated Au NPs.[5] An accompanying range of research spread generally into other nanoparticle properties: photoluminescence,[6] clusters of nanoparticles,[7] biological properties,[8] and catalytic properties.[9]

The $Au_{25}L_{18}$ NP emerged as an interesting target: obvious molecule-like properties, synthetic accessibility, and isolation with good monodispersity. Its small size was appealing for theoretical investigations, which have played important roles. Analytical advances helped to settle its identity; it was initially mislabeled as $Au_{28}(SG)_{16}$ (SG = glutathione)[10,11] and as $Au_{38}(SCH_2CH_2Ph)_{24}$.[12] Tsukuda et al.[13] analyzed a series of electrophoretically fractionated NPs by electrospray ionization mass spectrometry (ESI-MS) and relabeled the glutathione-protected NP as $Au_{25}(SG)_{18}$. In the intervening periods, several works had been published mislabeling the NPs as Au_{38} and Au_{28}.

Tracy et al.[14,15] established by high-resolution ESI-MS that the Au_{38} NP was an anionic species: $Au_{25}(SCH_2CH_2Ph)_{18}^-$. This was accented by a structure determination[16] of the salt, $[Oct_4N^+][Au_{25}(SCH_2CH_2Ph)_{18}^-]$, that serendipitously coincided with a concurring DFT prediction.[17] This breakthrough revealed a protecting ligand shell (Figure 1) very different from the thiolate "head-down" ligand bonding inferred[5] by analogy with SAMs on planar Au(111) surfaces. The NP core is a (slightly) distorted Au_{13} centered icosahedron surrounded by six $Au_2(SR)_3$ semirings, giving three kinds of Au sites (center, icosahedral surface, and semiring) and two thiolate environments. A subsequent crystal structure[18] of the oxidized form ($Au_{25}(SCH_2CH_2Ph)_{18}^0$) revealed a structural difference between the protecting semirings in the oxidized neutral and native anionic forms.

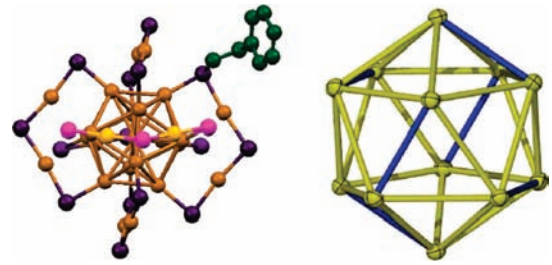

FIGURE 1. (left) X-ray crystal structure of $[Oct_4N^+][Au_{25}(SCH_2CH_2Ph)_{18}^-]$.[16] The icosahedral Au_{13} core is surrounded by six $Au_2(SR)_3$ semirings, which are slightly puckered in the reduced nanoparticle as shown for the semiring with more pronounced yellow and pink colors. (right) The icosahedral Au_{13} core (minus the center Au) is slightly distorted; the blue Au−Au bonds lying directly below the center of each semiring are on average 0.12 Å shorter than the yellow Au−Au bonds (average 2.96 Å). Overall Au−Au average 2.93 Å. Au_{13} core diameter 9.8 Å; overall nanoparticle diameter 23.9 Å. Data and figure from ref 16.

The semiring structures in Figure 1 were not a complete surprise. Somewhat earlier, Kornberg et al.[19] reported the structure of a $Au_{102}(SPh\text{-}p\text{-}CO_2H)_{44}$ NP capped by shorter -SR-Au-SR- semirings ("staples"), supporting earlier work by the Häkkinen group[20] proposing that semiring protecting structures could be involved in the thiolate chemistry of Au NPs. Au NP research thus arrived at an informative confluence of experiment and theory, a striking feature of which is the semiring protecting ligand layer seen in Figure 1.

Other interesting aspects of $Au_{25}L_{18}$ are found in its voltammetry, optical spectra and photoluminescence, electron transfer chemistry, and mass spectrometry. This Account will expand on these and other observations.

Synthesis

Early syntheses of water-soluble glutathione-protected NPs by the Whetten[10] and Tsukuda[11,13] groups involved adding excess aqueous sodium borohydride to a cooled (0 °C) methanolic mixture of $HAuCl_4$ and glutathione. The methanol-washed, polydisperse brown-black precipitate was size-fractionated by polyacrylamide gel electrophoresis. This procedure, while pivotal in early investigations, was burdened by low yields, product polydispersity, and lengthy fractionation.

Our initial synthesis[12] of the organic-soluble $Au_{25}(SCH_2CH_2Ph)_{18}$ nanoparticle used a modified version of the "Brust reaction";[2] $AuCl_4^-$ is phase-transferred from water to toluene, reacted with $HSCH_2CH_2Ph$, and then reduced by adding aqueous $NaBH_4$. The $[Oct_4N^+][Au_{25}(SCH_2CH_2Ph)_{18}^-]$ nanoparticle product is fortuitously extractable by acetonitrile, as confirmed by (initially[12]) UV−vis and ^1H NMR, and (later[14]) mass spectrometry, with a yield of ∼15%.

Further procedural improvements[21,22] have increased the yield of the $-SCH_2CH_2Ph$ protected NP. Wu et al.[21] enhanced the yield to ca. 40% by tuning the temperature and duration of different steps, hypothesizing that reduced temperature and prolonged slow stirring increases the Au(I)/SR aggregates leading to Au_{25} clusters. In our own hands, this procedure produces oxidized NPs (Au_{25}^0), so we modified[23] it to avoid this effect. It is now possible to produce substantial quantities (>500 mg per preparation, ca. 50% yield based on Au) of pure Au_{25}^- NP with $-SCH_2CH_2Ph$ and with several other thiolate ligands.

The ligand shell of $Au_{25}L_{18}^-$ can be altered, partially[24] or completely,[25] by ligand exchanges, which have been valuable tools in exploring NP properties.[5] Characterized as associative reactions,[26] they are first-order in NP and incoming thiol. It is evident from Figure 1 that exchange of ligands on the semirings must involve breaking multiple Au−SR bonds, but the details of this reaction remain unclear.

Crystal Structure

A seminal step in understanding small Au nanoparticles was the report[19] of the "staple" coordination geometry of the thiolate ligands on the NP $Au_{102}(SPh\text{-}p\text{-}CO_2H)_{44}$. Shortly later, the structures[16,18] were also solved for the two redox states of Au_{25} (−1 then 0). While earlier predictions[27,28] regarding the Au_{25} structure were not supported experimentally, DFT calculations published concurrently[17] with the Au_{25}^- crystal result correctly represented the main structural details, including the semirings (Figure 1). Nuances of these crystal structures led to theoretical predictions regarding the structure of other sizes of nanoparticles, including $Au_{38}(SR)_{24}$,[29] for which theoretical structure predictions[30a,b] have seen experimental support.[30c]

The $[Oct_4N^+][Au_{25}(SCH_2CH_2Ph)_{18}^-]$ crystal has a triclinic space group *P*1 and unit cell with $Z = 1$, three different Au sites (centered, Au_{13} surface, semiring), and six semirings. The thiolate sulfur has two different environments, and the nearly linear −S−Au−S− coordination geometries are reminiscent of Au(I) chemistry. Au−Au distances within the Au_{13} core are typical for Au−Au atom bonding.[16] Both the icosahedron and the semirings are slightly distorted; core Au−Au bonds lying below the semiring centers (Figure 1, right) are slightly shorter than the others. In the semirings, the terminal Au_{CORE}−S bonds are slightly longer (2.38 Å) than the others (2.32 Å), and the semirings are slightly puckered. These observations suggest an intimate structural relationship between the ligands and the core. DFT calculations assessing the high Au_{25} stability[17] concluded that the HOMO level is 3-fold degenerate and mainly P-character while the LUMO level is 2-fold degenerate with mainly D-symmetry. The energy gap is predicted as 1.2 eV, which is close to the experimental 1.3 eV.[31] The Au_{13} core contains 14 valence electrons, the electronic density of states reveals a shell closing at 8 electrons, so the semirings localize one Au(6s) electron each via the formation of strongly polar covalent bonds. As a "monolayer protected cluster,"[5] the six bidentate entities $Au_2(SR)_3$ constitute the monolayer of protecting ligand.

The crystal structure of the oxidized NP, $Au_{25}(SCH_2CH_2Ph)_{18}^0$, reported by Zhu et al.,[18] differs from that in Figure 1 in (at least) one major respect; the semirings are flattened. The structural difference between the two redox states implies that the electron transfer energy barrier includes an inner sphere reorganizational component, which had been inferred in earlier reports.[32−34]

Mass Spectrometry

Many ionization modes have been applied in NP MS analysis, including Cf plasma desorption ionization,[35] laser desorption ionization (LDI),[10,22,36] and ESI.[11,13,37] ESI-MS is an attractive, low-fragmentation mode and was employed in the first correct compositional assignment of $Au_{25}L_{18}$ by Negishi et al.[13] using electrophoretically separated water-soluble NPs with glutathione ligands. Implementing higher resolution positive-mode ESI-MS, Tracy et al.[14] used monodisperse methoxy penta(ethylene glycol) thiolate ligands ($-S-(C_2H_4O)_5CH_3$, −S−PEG) in the $Au_{25}L_{18}^-$ ligand shell to coordinate with alkali metal ions, producing 3+ and 4+ NP charge states (Figure 2a). The envelopes of these states contain major peaks spaced by 130 Da (the mass difference between −S−PEG and $-SCH_2CH_2Ph$) that represent different numbers of exchange-incorporated −S−PEG ligands at the time of sampling. The 3+ ion spectra (Figure 2b) using Na^+ and Cs^+ salts are accurately reconciled by assuming −S−PEG coordination of four Na^+ or Cs^+, which concurrently reveals the nanoparticle as reduced and present as the $[Oct_4N^+][Au_{25}(SCH_2CH_2Ph)_{18}^-]$ salt. The ESI-MS analysis[15a] was expanded to other ligands (See Supporting Information Figures S-1 and S-2), revealing a rich chemistry of ligand dissociation, fragmentation, and adduct formation. These results coincide with and sharpen the isolation and "magic stability" characterization of the $Au_{25}L_{18}$ NP by Tsukuda et al.[38] Lessons learned in the ESI-MS analysis of Au_{25} have been important in extending exact ESI-MS analysis to higher mass NPs like $Au_{144/146}$.[15b]

Matrix-assisted laser desorption ionization (MALDI-MS) and LDI[10,22,36,37] used in NP investigations typically yield extensive core and ligand fragmentation, complicating formula assignments. A change from typical proton-transfer matrices to

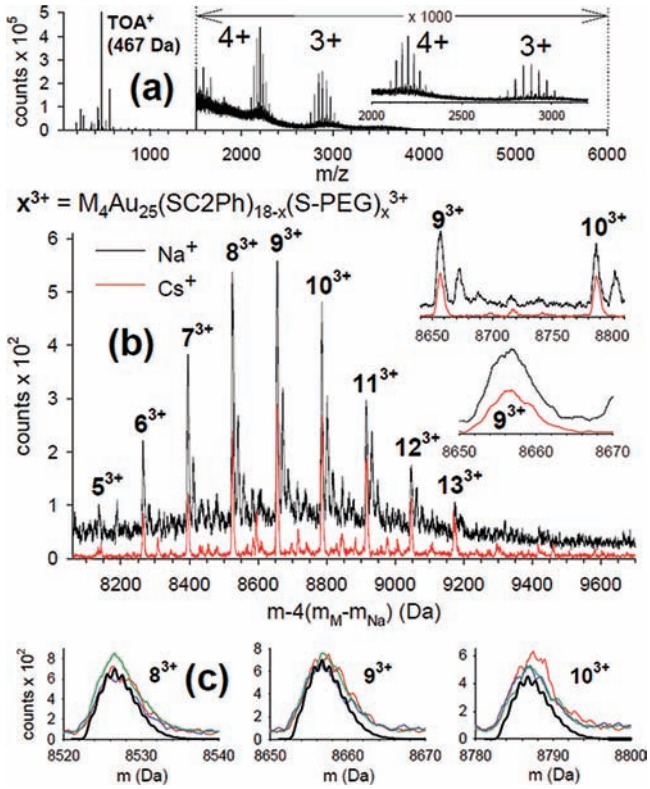

FIGURE 2. (a) Full ESI scan of $Au_{25}L_{18}$ with additional NaOAc. (b) Set of 3+ peaks acquired by adding NaOAc (black) and CsOAc (red) to the NP solution before spraying. Insets show greater detail in selected regions. (c) High-resolution analysis of prominent 3+ ions acquired in the NaOAc experiments compared with simulations (black). Reproduced from ref 14. Copyright 2007 American Chemical Society.

one reputedly favoring electron-transfer and use of threshold low laser fluences produced[39] unfragmented $Au_{25}(SCH_2CH_2Ph)_{18}$ spectra (Supporting Information, Figure S-3). A favored loss of a stable fragment Au_4L_4 forecasts an eventual better understanding of NP fragmentation chemistry.

The MALDI study,[39] and another (Supporting Information, Figure S-4) using fast atom bombardment (FAB) ionization,[40] stimulated a more explicit examination[41] by collision-induced dissociation (CID MS/MS) of −S−PEG exchanged Au_{25} NP ions generated in ESI-MS. In this ion trap-based experiment, selected precursor ions collide with Ar gas and the resulting fragments are mass analyzed (Supporting Information, Figure S-5). The detected low-mass fragments include not only the loss of an entire semiring fragment Au_2SR_3, but also loss of a $Au_4(SR)_4$ moiety, which requires a rearrangement process involving more than one semiring. Under non-CID conditions, ESI-TOF-MS and ESI-FTICR-MS spectra (Supporting Information, Figure S-6) display the same small fragments at isotopic resolution. The CID results demonstrate that the small fragments are a consequence of the ESI process as opposed to contaminants in the NP samples. Some high mass fragments in the CID could be understood (such as $Au_{24}L_{16}$, indicating a AuL_2 loss, Supporting Information, Figure S-7), but other nonobvious high mass fragments show that $Au_{25}L_{18}$ NP fragmentation chemistry is apparently multistep and includes rearrangements.

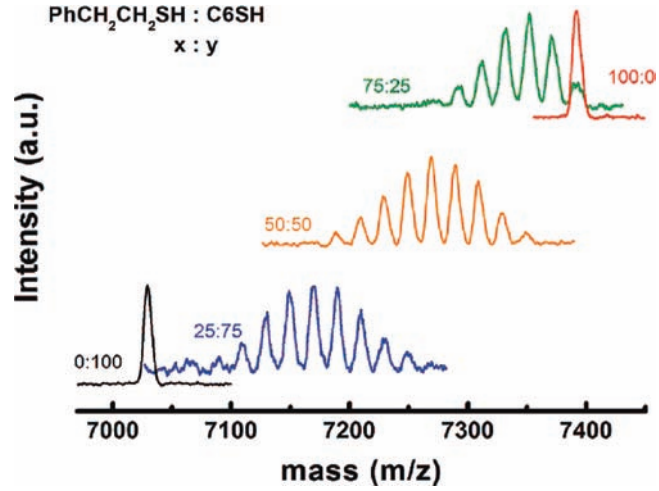

FIGURE 3. Monolayer ligand distribution of the mixed Brust reaction product $Au_{25}(SCH_2CH_2Ph)_{18-x}(SC6)_x$ as observed by MALDI-MS spectrum using different starting ligand mole ratios 25:75, 50:50, and 75:25. Reproduced from ref 42. Copyright 2008 American Chemical Society.

The envelopes of 3+ and 4+ peaks (Figure 2a) have further interest because the distribution of peak intensities (and relative nanoparticle populations thus represented) is related to whether ligand exchanges occur randomly and independently (of one another) over the 18 −SR binding sites on $Au_{25}L_{18}$. This was explored[42] using MALDI on NPs synthesized with different mole ratios of hexanethiol and phenylethanethiol (Figure 3). In each mixed-ligand nanoparticle, the relative numbers of hexanethiolate and phenylethanethiolate ligands follow the expected binominal distribution (as in Figure 2). The overall process, however, does favor a greater *average* incorporation of the phenylethanethiolate ligand as is clear from the central average of the peak distribution for the 50:50 starting ligand ratio.

Mixed ligand distributions can also be observed[42] as they develop during a ligand exchange reaction (like Figure 2). Statistically analyzing the profile of ligand exchange incorporation of −SC6 ligands onto $Au_{25}(SCH_2CH_2Ph)_{18}$ produces the binomial distribution expected for the 18 ligand sites having identical and independent reactivities. However, distributions from exchange of −SPh ligands were narrower than expected. It would appear that such ligand exchange data could be valuable in assessing intrananoparticle ligand interactions,[42] such as those invoked in phase-segregated ligand shells.[43]

ESI-MS data were also useful for studying M_{25} bimetal nanoparticles synthesized[44] using a mixture of Au and Pd salts with the $HSCH_2CH_2Ph$ thiol and an isolation procedure targeting small NP products. Exchanges to introduce −S−PEG ligands and allow positive mode ESI-MS spectra (Supporting Information, Figure S-8) revealed that the product was a mixture of $Au_{25}(SCH_2CH_2Ph)_{18}$ and $Au_{24}Pd(SCH_2CH_2Ph)_{18}$. Larger numbers of introduced Pd sites were not observed. Substitution of Pd for Au in $Au_{25}(SR)_{18}$ evidently is not favorable or produces nanoparticles unstable at the M_{25} size. That introduction[44] of a single Pd atom substantially alters the distinctive $Au_{25}L_{18}$ optical and electrochemical signatures was supported by a DFT study,[45] concluding that the optical properties and energy gap differ according to the location of the Pd site (center, core surface, semiring) and that inclusion of additional Pd sites could lead to more readily oxidizable and less stable materials. DFT efforts[46,47] have also considered the possibilities of a wider range of (singly) incorporated elements, and it seems possible that the properties of $Au_{25-x}M_xL_{18}$ nanoparticles could be "tuned" in this way.

Voltammetry and Electron Transfer Properties

The voltammetry of small Au nanoparticles can be very informative about their electronic properties. Nanoparticles of "Au_{144}" and "Au_{225}" composition show, because of having exceedingly small individual double layer capacitances,[48] quantized double layer charging where the voltage spacing between neighboring voltammetric features is more or less uniform and dominated by capacitive properties. Even smaller nanoparticles show an extra voltage spacing (the electrochemical energy gap) between the first oxidation and first reduction steps, which reflects the emergence of a HOMO−LUMO energy gap.[48] The gap between the formal potentials of the $Au_{25}L_{18}^{0/1-}$ and $Au_{25}L_{18}^{1-/2-}$ couples (in CH_2Cl_2/electrolyte) is[31] 1.62 V (Figure 4). Estimating charging energy from the spacing between the formal potentials of the $Au_{25}L_{18}^{0/1-}$ and $Au_{25}L_{18}^{1+/0}$ waves (0.29 V) gives a gap energy that is in agreement with the optically observed HOMO−LUMO gap energy of 1.33 eV.

The formal potential of the $Au_{25}L_{18}^{0/1-}$ couple (HOMO electronic level) is very sensitive to the thiolate ligand employed. Replacing[25] the original $-SCH_2CH_2Ph$ ligands with thiophenolate ligands (−SPh-*p*-X, where X = NO_2, Br, H, CH_3, and OCH_3) shifts the formal potential positively as "X" becomes more electron-withdrawing, without change in the HOMO−LUMO gap energy. The ligand exchange kinetics follow an analogous order,[26] with $-NO_2$ being the fastest. It has been further found, experimentally and with DFT calculations,[24] that the $Au_{25}L_{18}^{0/1-}$ formal potential changes *linearly* with the number of exchanged ligands: 42 mV/ligand for exchange by $-SPhNO_2$ and 60 mV/ligand for (theoretical) exchange by $-SCH_2Cl$. Importantly, the DFT analysis shows that the ligand-induced transfer of charge occurs solely within the semiring structure (Figure 1) and not within the Au_{13} core.

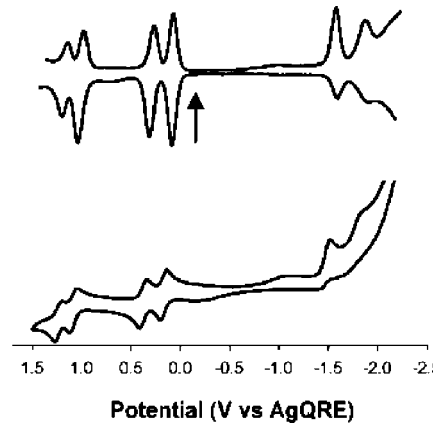

FIGURE 4. (top) Differential pulse voltammogram (DPV) at 0.02 V/s, and (bottom) cyclic voltammogram (0.1 V/s) of $Au_{25}(SCH_2CH_2Ph)_{18}$ in 0.1 M Bu_4NPF_6 in degassed CH_2Cl_2 at 0.4 mm diameter Pt working, Ag quasi-reference (AgQRE), and Pt-wire counter electrodes. Both voltammograms were obtained at −70 °C. Arrow indicates solution rest potentials. Reproduced from ref 31. Copyright 2004 American Chemical Society.

Considerable information is also now available regarding the dynamics of electron transfers in the $Au_{25}(SCH_2CH_2Ph)_{18}^{0/1-}$ redox couple. The electron-hopping conductivities (which reflect electron self-exchange rates) of mixed valent films[33] of $Au_{25}^{0/1-}$ and $Au_{144}^{1+/0}$ are remarkably different, the former being $>10^3$ slower. The activation barrier energies also differ sharply, by 3-fold. Estimates[33] of the outer-sphere (Marcus) reorganizational energies for these two nanoparticle couples are both close to the experimental $Au_{144}^{1+/0}$ nanoparticle result, suggesting that the slow $Au_{25}^{0/1-}$ electron transfers reflect an "inner sphere" reorganizational energy barrier[49] component, that is, changes in nuclear coordinates accompany electron transfer. Values of heterogeneous electron transfer rate constants and activation barrier energies in solution voltammetry reported by Antontello et al.[24] supported that suggestion.

In a ^1H NMR investigation[32] of the $Au_{25}(SCH_2CH_2Ph)_{18}^{0/1-}$ electron transfer couple, and following the structural elucidation[16] of the reduced form, $Au_{25}(SCH_2CH_2Ph)_{18}^{1-}$, the chemical shift of the α-methylene proton resonances in solutions of solely the oxidized form was found to lie about 2 ppm downfield from that of the reduced form. The large chemical shift

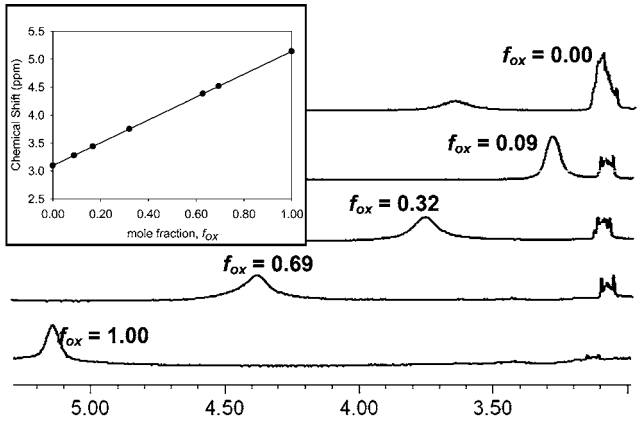

FIGURE 5. ^{1}H Nuclear magnetic resonance spectra of reduced $[Au_{25}(SCH_2CH_2)_{18}]^{1-}$, oxidized $[Au_{25}(SCH_2CH_2)_{18}]^0$, and mixtures of the two forms, presented as fraction of oxidized (f_{ox}) material present. The inset shows the linearity of chemical shift with f_{ox}, consistent with a fast exchange mechanism. The mixtures exhibit peak widths greater than those of the two pure forms. The fwhm is dependent on the total concentration of nanoparticle in solution and the relative fraction of each form. Reproduced from ref 32. Copyright 2008 American Chemical Society.

change is recognized as a consequence of an unpaired electron spin in the $Au_{25}(SCH_2CH_2Ph)_{18}^0$ nanoparticle, and indeed its electron spin resonance spectrum has since been re-ported.[50] Mixtures of $Au_{25}(SCH_2CH_2Ph)_{18}^{1-}$ and $Au_{25}(SCH_2CH_2Ph)_{18}^0$ show averaged chemical shifts[32] as expected for electron exchanges between the two states (Figure 5) and display an enhanced line width broadening, which reflects a classical NMR two-state exchange process. Its analysis and temperature dependence produced[32] a room temperature electron self-exchange rate constant $k_{EX} = 3 \times 10^7$ M^{-1} s^{-1} and a large activation energy (25 kJ/mol) that is consistent with the earlier results.[33,34] The suggestion[33] of a structural change accompanying electron transfer was confirmed by Raman spectroscopy; the Au−S stretch energies (now recognized as radial breathing modes[51]) of the ligand shell differ by 24 cm^{-1} between the two states. A further piece of the electron transfer dynamics puzzle was added by solution[18] of the oxidized form's crystal structure, which showed that the "puckered" semirings of the reduced form become flattened upon oxidation. An alternative theoretical view[51] suggests that the ring puckering may originate from interactions with the Oct_4N^+ counterion. The structural change indicated by the Raman result may possibly therefore be a different, more complex structural alteration, or the resolution of the theory does not cope with a small puckering change.

The preceding analysis of structural aspects of the $Au_{25}(SCH_2CH_2Ph)_{18}^{0/1-}$ electron transfer couple dynamics, to which a variety of different experiments contributed, is the first nanoparticle analogy to the classical "inner sphere reorganization" in slowed electron transfers of the $Fe(H_2O)_6^{3+/2+}$ couple where the Fe−O bond length contracts in the oxidized form.[49]

Optical Spectroscopy

Au_{25} nanoparticles exhibit interesting optical absorbance and fluorescence characteristics. The optical dependence[31] on oxidation state of $Au_{25}(SCH_2CH_2Ph)_{18}$ is illustrated in Supporting Information, Figure S-9. The broad feature around 1.8 eV for the reduced state is two overlapped peaks (1.84 eV (675 nm) and 1.61 eV (770 nm)), the latter of which is extinguished upon oxidation and reflects a HOMO electron. The absorbance edge from these spectra, 1.33 eV, matches the electrochemical observations and is close to the 1.24 eV calculated[17] value. Calculations on these low-energy optical transitions[17,52,53] have been consistent with the idea[54] of "superatomic orbitals" of the NP core.

Au_{25} nanoparticles exhibit near-IR photoluminescence (PL), weakly[31] with $-SCH_2CH_2Ph$ ligands but more intensely with electron-withdrawing ones.[6,55] The PL is attributed to surface states since its energy is essentially invariant with the size of the nanoparticle.[56] The later discovery[16] of the semiring ligand architecture invites attention to it as the probable electronic locus of these emissions.

Attention is also turning to transient optical spectroscopy to map the dynamics of electronic relaxations. Upon excitation at 530 nm on fast time scales, pump−probe experiments show very fast (<0.2 ps) relaxation of the core excitation with internal conversion to ligand shell states, which relax on a slower, 1.2 ps, time scale. The NIR PL of Au_{25} NPs has been determined by transient absorption to occur with lifetimes of 3 ps[57] and 4−5 ps.[58] Goodson and co-workers observed[59] two-photon cross sections for Au_{25} NPs and found them much larger than those of organic macromolecules and semiconductor nanocrystals. Two photon absorptions can have a number of useful nonlinear optical applications in biological imaging, optical power limiting, and nanolithography. Au_{25} has also been shown to be an effective material for fluorescence resonance energy transfer (FRET)[60] between the core and ligand shell, specifically in the case of $Au_{25}(SG)_{18}$ and dansyl chromophores bound to the core via glutathione linkers. Efficient FRET was observed from the dansyl donor to the Au_{25} core, as observed by the reduced lifetime of the excited state and reduced fluorescence of the dansyl chromophore ligand. Concurrently, the Au_{25} emission at 700 nm was enhanced, which is consistent with FRET observations.

Conclusion

We report on what has become perhaps the most understood Au nanoparticle and track it through its history of (incorrect and correct) identification, structure determination, and analytical properties. As the details of Au_{25} continue to be fleshed out, we believe the results summarized in this Account will be useful for further analyses and applications. In the meantime, we also hope that the story of this nanoparticle will be of pedagogical value to those who teach about nanoparticle science.

This research was supported by the National Science Foundation and Office of Naval Research. We also thank the many researchers, past and present, who have contributed to the advancement of the materials mentioned in this Account.

Supporting Information Available. Supplementary experimental data and references to papers not discussed above. This material is available free of charge via the Internet at http://pubs.acs.org.

BIOGRAPHICAL INFORMATION

Joseph F. Parker (01/23/1983, from Atlanta, GA) was educated at the Georgia Institute of Technology (B.S., 2004) under the guidance of Professor L. A. Bottomley and the University of North Carolina at Chapel Hill (Ph.D. analytical chemistry, 2010) working under Professor Murray. He was the recipient of the ACS Undergraduate Award in Analytical Chemistry, was awarded a summer scholarship at the NASA Langley Aerospace Research Center, and is currently a member of the American Chemical Society.

Christina A. Fields-Zinna (11/18/1982, from Lumberton, NC) attended Harvard University (B.A., 2005) and the University of North Carolina at Chapel Hill (Ph.D., analytical chemistry, 2010). Some of her notable achievements are the Gates' Millennium Scholarship and the fourth Annual Schering-Plough Science and Innovation Award. She has currently accepted a forensic toxicologist position with the Georgia Bureau of Investigation.

Royce W. Murray (01/09/1937, from Birmingham, AL) was educated at Birmingham Southern College (B.S., 1957) and Northwestern University (Ph.D., analytical chemistry, 1960). He is Kenan Professor of Chemistry and is celebrating his 50th year as an active teacher and scholar, having published over 450 research papers. He is a member of the National Academy of Sciences and is Editor of the ACS journal *Analytical Chemistry*.

FOOTNOTES

*To whom correspondence should be addressed. rwm@email.unc.edu.

REFERENCES

1 Rose, N. L.; Mirkin, C. A. Nanostructures and Biodiagnostics. *Chem. Rev.* **2005**, *105*, 1547–1562.

2 Brust, M.; Walker, M.; Bethell, D.; Schiffrin, D. J.; Whyman, R. Synthesis of Thiol-Derivatised Gold Nanoparticles in a Two-Phase Liquid-Liquid System. *J. Chem. Soc., Chem. Commun.* **1994**, 801–802.

3 Whetten, R. L.; Khoury, J. T.; Alvarez, M. M.; Murthy, S.; Vezmar, I.; Wang, Z. L.; Stephens, P. W.; Cleveland, C. L.; Luedtke, W. D.; Landman, U. Nanocrystal Gold Molecules. *Adv. Mater.* **1996**, *8*, 428–433.

4 Terrill, R. H.; Postlethwaite, T. A.; Chen, C.-h.; Poon, C.-D.; Terzis, A.; Chen, A.; Hutchison, J. W.; Clark, M. R.; Wignall, G.; Londono, J. D.; Superfine, R.; Falvo, M.; Johnson, C. S.; Samulski, E. T.; Murray, R. W. Monolayers in Three Dimensions: NMR, SAXS, Thermal, and Electron Hopping Studies of Alkanethiol Stabilized Gold Clusters. *J. Am. Chem. Soc.* **1995**, *117*, 12537–12548.

5 Templeton, A. C; Wuelfing, W. P.; Murray, R. W. Monolayer-Protected Cluster Molecules. *Acc. Chem. Res.* **2000**, *33*, 27–36.

6 Wang, G.; Huang, T.; Murray, R. W.; Menard, L.; Nuzzo, R. G. Near-IR Luminescence of Monolayer-Protected Metal Clusters. *J. Am. Chem. Soc.* **2005**, *127*, 812–813.

7 McConnell, W. P.; Novak, J. P.; Brousseau, L. C., III; Fuierer, R. R.; Tenent, R. C.; Feldheim, D. L. Electronic and Optical Properties of Chemically Modified Metal Nanoparticles and Molecularly Bridged Nanoparticle Arrays. *J. Phys. Chem. B* **2000**, *104*, 8925–8930.

8 Andres, R. P.; Bein, T.; Dorogi, M.; Feng, S.; Henderson, J. I.; Kubiak, C. P.; Mahoney, W.; Osifchin, R. G.; Reifenberger, R. "Coulomb Staircase" at Room Temperature in a Self-Assembled Molecular Nanostructure. *Science* **1996**, *272*, 1323–1325.

9 Pasquato, L.; Pengo, P.; Scrimin, P. Functional Gold Nanoparticles for Recognition and Catalysis. *J. Mater. Chem.* **2004**, *14*, 3481–3487.

10 Schaaff, T. D.; Knight, G.; Shafigullin, M. N.; Borkman, R. F.; Whetten, R. L. Isolation and Selected Properties of a 10.4 kDa Gold:Glutathione Cluster Compound. *J. Phys. Chem. B* **1998**, *102*, 10643–10646.

11 Negishi, Y.; Takasugi, Y.; Sato, S.; Yao, H.; Kimura, K.; Tsukuda, T. Magic-Numbered Au_n Clusters Protected by Glutathione Monolayers ($n = 18$, 21, 25, 28, 32, 39): Isolation and Spectroscopic Characterization. *J. Am. Chem. Soc.* **2004**, *126*, 6518–6519.

12 Donkers, R. L.; Lee, D.; Murray, R. W. Synthesis and Isolation of the Molecule-like Cluster $Au_{38}(SCH_2CH_2Ph)_{24}$. *Langmuir* **2004**, *20*, 1945–1952.

13 Negishi, Y.; Nobusada, K.; Tsukuda, T. Glutathione-Protected Gold Clusters Revisited: Bridging the Gap between Gold(I)-Thiolate Complexes and Thiolate-Protected Gold Nanocrystals. *J. Am. Chem. Soc.* **2005**, *127*, 5261–5270.

14 Tracy, J. B.; Kalyuzhny, G.; Crowe, M. C.; Balasubramanian, R.; Choi, J.-P.; Murray, R. W. Poly(ethylene glycol) Ligands for High-Resolution Nanoparticle Mass Spectrometry. *J. Am. Chem. Soc.* **2007**, *129*, 6706–6707.

15 (a) Tracy, J. B.; Crowe, M. C.; Parker, J. F.; Hampe, O.; Fields-Zinna, C. A.; Dass, A.; Murray, R. W. Electrospray Ionization Mass Spectrometry of Uniform and Mixed Monolayer Nanoparticles: $Au_{25}[S(CH_2)_2Ph]_{18}$ and $Au_{25}[S(CH_2)_2Ph]_{18-x}(SR)_x$. *J. Am. Chem. Soc.* **2007**, *129*, 16209–16215. (b) Fields-Zinna, C. A.; Sardar, R.; Beasley, C. A.; Murray, R. W. Electrospray Ionization Mass Spectrometry of Intrinsically Cationized Nanoparticles, $[Au_{144/146}(SC_{11}H_{22}N(CH_2CH_3)_3^+)_x(S(CH_2)_5CH_3)_y]^{x+}$. *J. Am. Chem. Soc.* **2009**, *131*, 13844–13851.

16 Heaven, M. W.; Dass, A.; White, P. S.; Holt, K. M.; Murray, R. W. Crystal Structure of the Gold Nanoparticle $[N(C_8H_{17})_4][Au_{25}(SCH_2CH_2Ph)_{18}]$. *J. Am. Chem. Soc.* **2008**, *130*, 3754–3755.

17 Akola, J.; Walter, M.; Whetten, R. L.; Häkkinen, H.; Grönbeck, H. On the Structure of Thiolate-Protected Au_{25}. *J. Am. Chem. Soc.* **2008**, *130*, 3756–3757.

18 Zhu, M.; Eckenhoff, W. T.; Pintauer, T.; Jin, R. Conversion of Anionic $[Au_{25}(SCH_2CH_2Ph)_{18}]^-$ Cluster to Charge Neutral Cluster via Air Oxidation. *J. Phys. Chem. C* **2008**, *112*, 14221–14224.

19 Jadzinsky, P. D.; Calero, G.; Ackerson, C. J.; Bushnell, D. A.; Kornberg, R. D. Structure of a Thiol Monolayer-Protected Gold Nanoparticle at 1.1 Å Resolution. *Science* **2007**, *318*, 430–433.

20 Häkkinen, H.; Walter, M.; Grönbeck, H. Divide and Protect: Capping Gold Nanoclusters with Molecular Gold−Thiolate Rings. *J. Phys. Chem. B* **2006**, *110*, 9927–9931.

21 Wu, Z.; Suhan, J.; Jin, R. One-Pot Synthesis of Atomically Monodisperse, Thiol-Functionalized Au_{25} Nanoclusters. *J. Mater. Chem.* **2009**, *19*, 622–626.

22 Price, R. C.; Whetten, R. L. All-Aromatic, Nanometer-Scale, Gold-Cluster Thiolate Complexes. *J. Am. Chem. Soc.* **2005**, *127*, 13750–13751.

23 Parker, J. F.; Weaver, J. E. F.; McCallum, F.; Fields-Zinna, C. A.; Murray, R. W. *Langmuir* **2010**, submitted.

24 Parker, J. F.; Kacprzak, K. A.; Lopez-Acevedo, O.; Hakkinen, H.; Murray, R. W. Experimental and Density Functional Theory Analysis of Serial Introductions of Electron-Withdrawing Ligands into the Ligand Shell of a Thiolate-Protected Au25 Nanoparticle. *J. Phys. Chem. C* **2010**, *114*, 8276–8281.

25 Guo, R.; Murray, R. W. Substituent Effects on Redox Potentials and Optical Gap Energies of Molecule-like $Au_{38}(SPhX)_{24}$ Nanoparticles. *J. Am. Chem. Soc.* **2005**, *127*, 12140–12143.

26 Guo, R.; Song, Y.; Wang, G.; Murray, R. W. Does Core Size Matter in the Kinetics of Ligand Exchanges of Monolayer-Protected Au Clusters? *J. Am. Chem. Soc.* **2005**, *127*, 2752–2757.

27 Iwasa, T.; Nobusada, K. Theoretical Investigation of Optimized Structures of Thiolated Gold Cluster $[Au_{25}(SCH_3)_{18}]^+$. *J. Phys. Chem. C* **2007**, *111*, 45–49.

28 Iwasa, T.; Nobusada, K. Gold-Thiolate Core-in-Cage Cluster $Au_{25}(SCH_3)_{18}$ Shows Localized Spins in Charged States. *Chem. Phys. Lett.* **2007**, *441*, 268–272.

29 (a) Jiang, D.; Tiago, M. L.; Luo, W.; Dai, S. The "Staple" Motif: A Key to Stability of Thiolate-Protected Gold Nanoclusters. *J. Am. Chem. Soc.* **2008**, *130*, 2777–2779. (b) Jiang, D.; Luo, W.; Tiago, M. L.; Dai, S. In Search of a Structural Model for a Thiolate-protected Au_{38} Cluster. *J. Chem. Phys. C* **2008**, *112*, 13905–13910.

30 (a) Pei, Y.; Gao, Y.; Zeng, X. C. Structural Prediction of Thiolate-Protected Au_{38}: A Face-Fused Bi-icosahedral Au Core. *J. Am. Chem. Soc.* **2008**, *130*, 7830. (b) Lopez-Acevedo, O.; Tsunoyama, H.; Tsukuda, T.; Hakkinen, H.; Aikens, C. M. Chirality and Electronic Structure of the Thiolate-Protected Au_{38} Nanocluster. *J. Am. Chem. Soc.* **2010**, *132*, 8210–8218. (c) Huifeng Qian, H.; Eckenhoff, W. T.; Zhu, Y.; Pintauer, T.; Jin, R. Total Structure Determination of Thiolate-Protected Au_{38} Nanoparticles. *J. Am. Chem. Soc.* **2010**, *132*, 8280–8281.

31 Lee, D.; Donkers, R. L.; Wang, G.; Harper, A. S.; Murray, R. W. Electrochemistry and Optical Absorbance and Luminescence of Molecule-like Au_{38} Nanoparticles. *J. Am. Chem. Soc.* **2004**, *126*, 6193–6199.

32 Parker, J. F.; Choi, J.-P.; Wang, W.; Murray, R. W. Electron Self-Exchange Dynamics of the Nanoparticle Couple $[Au_{25}(SC_2Ph)_{18}]^{0/1-}$ by Nuclear Magnetic Resonance Line-Broadening. *J. Phys. Chem. C* **2008**, *112*, 13976–13981.

33 Choi, J.-P.; Murray, R. W. Electron Self-Exchange between $Au_{140}{}^{+/0}$ Nanoparticles Is Faster Than That between $Au_{38}{}^{+/0}$ in Solid-State, Mixed-Valent Films. *J. Am. Chem. Soc.* **2006**, *128*, 10496–10502.

34 Antonello, S.; Holm, A. H.; Instuli, E.; Maran, F. Molecular Electron-Transfer Properties of Au_{38} Clusters. *J. Am. Chem. Soc.* **2007**, *129*, 9836–9837.

35 Fackler, J. P.; McNeal, C. J.; Winpenny, R. E. P.; Pignolet, L. H. Californium-252 Plasma Desorption Mass Spectrometry as a Tool for Studying Very Large Clusters; Evidence for Vertex-Sharing Icosahedra as Components of $Au_{67}(PPh_3)_{14}Cl_8$. *J. Am. Chem. Soc.* **1989**, *111*, 6434–6435.

36 Schaaff, T. G.; Shafigullin, M. N.; Khoury, J. T.; Vezmar, I.; Whetten, R. L. Properties of a Ubiquitous 29 kDa Au:SR Cluster Compound. *J. Phys. Chem. B* **2001**, *105*, 8785–8796.

37 (a) Negishi, Y.; Takasugi, Y.; Sato, S.; Yao, H.; Kimura, K.; Tsukuda, T. Kinetic Stabilization of Growing Gold Clusters by Passivation with Thiolates. *J. Phys. Chem. B* **2006**, *110*, 12218–12221. (b) Shichibu, Y.; Negishi, Y.; Tsukuda, T.; Teranishi, T. Large-Scale Synthesis of Thiolated Au_{25} Clusters via Ligand Exchange Reactions of Phosphine-Stabilized Au11 Clusters. *J. Am. Chem. Soc.* **2005**, *127*, 13464–13465.

38 Negishi, Y.; Chaki, N. K.; Shichibu, Y.; Whetten, R. L.; Tsukuda, T. Origin of Magic Stability of Thiolated Gold Clusters: A Case Study on $Au_{25}(SC_6H_{13})_{18}$. *J. Am. Chem. Soc.* **2007**, *129*, 11322–11323.

39 Dass, A.; Stevenson, A.; Dubay, G. R.; Tracy, J. B.; Murray, R. W. Nanoparticle MALDI-TOF Mass Spectrometry without Fragmentation: $Au_{25}(SCH_2CH_2Ph)_{18}$ and Mixed Monolayer $Au_{25}(SCH_2CH_2Ph)_{18-x}(L)_x$. *J. Am. Chem. Soc.* **2008**, *130*, 5940–5946.

40 Dass, A.; Dubay, G. R.; Fields-Zinna, C. A.; Murray, R. W. FAB Mass Spectrometry of $Au_{25}(SR)_{18}$ Nanoparticles. *Anal. Chem.* **2008**, *80*, 6845–6849.

41 Fields-Zinna, C. A.; Sampson, J. S.; Crowe, M. C.; Tracy, J. B.; Parker, J. F.; deNey, A. M.; Muddiman, D. C.; Murray, R. W. Tandem Mass Spectrometry of Thiolate-Protected Au Nanoparticles $Na_xAu_{25}(SC_2H_4Ph)_{18-y}(S(C_2H_4O)_5CH_3)_y$. *J. Am. Chem. Soc.* **2009**, *131*, 13844–13851.

42 Dass, A.; Holt, K.; Parker, J. F.; Feldberg, S. W.; Murray, R. W. Mass Spectrometrically Detected Statistical Aspects of Ligand Populations in Mixed Monolayer $Au_{25}L_{18}$ Nanoparticles. *J. Phys. Chem. C* **2008**, *112*, 20276–20283.

43 Jackson, A. M.; Hu, Y.; Silva, P. J.; Stellacci, F. From Homoligand- to Mixed-Ligand-Monolayer-Protected Metal Nanoparticles: A Scanning Tunneling Microscopy Investigation. *J. Am. Chem. Soc.* **2006**, *128*, 11135–11149.

44 Fields-Zinna, C. A.; Crowe, M. C.; Dass, A.; Weaver, J. E. F.; Murray, R. W. Mass Spectrometry of Small Bimetal Monolayer-Protected Clusters. *Langmuir* **2009**, *25*, 7704–7710.

45 Kacprzak, K. A.; Lehtovaara, L.; Akola, J.; Lopez-Acevedo, O.; Häkkinen, H. A Density Functional Investigation of Thiolate-Protected Bimetal $PdAu_{24}(SR)_{18}{}^z$ Clusters: Doping the Superatom Complex. *Phys. Chem. Chem. Phys.* **2009**, *33*, 7123–7129.

46 Jiang, D.; Da, S. From Superatomic $Au_{25}(SR)_{18}{}^-$ to Superatomic $M@Au_{24}(SR)_{18}{}^q$ Core-Shell Clusters. *Inorg. Chem.* **2009**, *48*, 2720–2722.

47 Walter, M.; Moseler, M. Ligand-Protected Gold Alloy Clusters: Doping the Superatom. *J. Phys. Chem. C* **2009**, *113*, 15834–15837.

48 Murray, R. W. Nanoelectrochemistry: Metal Nanoparticles, Nanoelectrodes, and Nanopores. *Chem. Rev.* **2008**, *108*, 2688–2720.

49 Zhang, D.; Liu, C. Reorganization Criteria and Their Effects on Inner-Sphere Barriers for Transition Metal Redox Pairs $M(H_2O)_6{}^{2+/3+}$(M=V, Cr, Mn, Fe and Co). *New J. Chem.* **2002**, *26*, 361–366.

50 Zhu, M.; Aikens, C. M.; Hendrich, M. P.; Gupta, R.; Qian, H.; Schatz, G. C.; Jin, R. Reversible Switching of Magnetism in Thiolate-Protected Au25 Superatoms. *J. Am. Chem. Soc.* **2009**, *131*, 2490–2492.

51 Akola, J.; Kacprzak, K. A.; Lopez-Acevedo, O.; Walter, M.; Grönbeck, H.; Häkkinen, H. Thiolate-Protected Au_{25} Superatoms as Building Blocks: Dimers and Crystals. *J. Phys. Chem. C*, published online Apr 27, **2010**, http://dx.doi.org/10/1021/jp1015438.

52 Zhu, M.; Aikens, C. M.; Hollander, F. J.; Schatz, G. C.; Jin, R. Correlating the Crystal Structure of A Thiol-Protected Au25 Cluster and Optical Properties. *J. Am. Chem. Soc.* **2008**, *130*, 5883–5885.

53 Aikens, C. M. Origin of Discrete Optical Absorption Spectra of $M_{25}(SH)_{18}{}^-$ Nanoparticles (M = Au, Ag). *J. Phys. Chem. C* **2008**, *112*, 19797–19800.

54 Walter, M.; Akola, J.; Lopez-Acevedo, O.; Jadzinsky, P. D.; Calero, G.; Ackerson, C. J.; Whetten, R. L.; Grönbeck, H.; Häkkinen, H. A Unified View of Ligand-Protected Gold Clusters As Superatom Complexes. *Proc. Natl. Acad. Sci. U.S.A.* **2008**, *105*, 9157–9162.

55 Wang, G.; Guo, R.; Kalyuzhny, G.; Choi, J.-P.; Murray, R. W. NIR Luminescence Intensities Increase Linearly with Proportion of Polar Thiolate Ligands in Protecting Monolayers of Au_{38} and Au_{140} Quantum Dots. *J. Phys. Chem. B* **2006**, *110*, 20282–20289.

56 Wang, G.; Huang, T.; Murray, R. W.; Menard, L.; Nuzzo, R. G. Near-IR Luminescence of Monolayer-Protected Metal Clusters. *J. Am. Chem. Soc.* **2005**, *127*, 812–813.

57 Varnavski, O.; Ramakrishna, G.; Kim, J.; Lee, D.; Goodson, T. Critical Size for the Observation of Quantum Confinement in Optically Excited Gold Clusters. *J. Am. Chem. Soc.* **2010**, *132*, 16–17.

58 Miller, S. A.; Womick, J. M.; Parker, J. F.; Murray, R. W.; Moran, A. M. Femtosecond Relaxation Dynamics of $Au_{25}L_{18}{}^-$ Monolayer-Protected Cluster. *J. Phys. Chem. C* **2009**, *113*, 9440–9444.

59 Ramakrishna, G.; Varnavski, O.; Kim, J.; Lee, D; Goodson, T. Quantum-Sized Gold Clusters as Efficient Two-Photon Absorbers. *J. Am. Chem. Soc.* **2008**, *130*, 5032–5033.

60 Muhammed, M. A. H.; Shaw, A. K.; Pal, S. K.; Pradeep, T. Quantum Clusters of Gold Exhibiting FRET. *J. Phys. Chem. C* **2008**, *112*, 14324–14330.